Cerebral organoids model human brain development and microcephaly

Published in final edited form as:
Nature. 2013 September 19; 501(7467): . doi:10.1038/nature12517.

Cerebral organoids model human brain development and microcephaly

Madeline A. Lancaster[1], **Magdalena Renner**[1], **Carol-Anne Martin**[2], **Daniel Wenzel**[1], **Louise S. Bicknell**[2], **Matthew E. Hurles**[3], **Tessa Homfray**[4], **Josef M. Penninger**[1], **Andrew P. Jackson**[2], and **Juergen A. Knoblich**[1]

[1]IMBA - Institute of Molecular Biotechnology of the Austrian Academy of Science, Vienna 1030, Austria

[2]MRC Human Genetics Unit, Institute of Genetics and Molecular Medicine, University of Edinburgh, Edinburgh, UK

[3]Wellcome Trust Sanger Institute, Cambridge, UK

[4]Department of Clinical Genetics, St. George's University, London, UK

Abstract

The complexity of the human brain has made it difficult to study many brain disorders in model organisms, and highlights the need for an *in vitro* model of human brain development. We have developed a human pluripotent stem cell-derived 3D organoid culture system, termed cerebral organoid, which develops various discrete though interdependent brain regions. These include cerebral cortex containing progenitor populations that organize and produce mature cortical neuron subtypes. Furthermore, cerebral organoids recapitulate features of human cortical development, namely characteristic progenitor zone organization with abundant outer radial glial stem cells. Finally, we use RNAi and patient-specific iPS cells to model microcephaly, a disorder that has been difficult to recapitulate in mice. We demonstrate premature neuronal differentiation in patient organoids, a defect that could explain the disease phenotype. Our data demonstrate that 3D organoids can recapitulate development and disease of even this most complex human tissue.

Introduction

Mammalian brain development begins with expansion of the neuroepithelium to generate radial glia (RG)[1]. These RGs divide at the apical surface within the ventricular zone (VZ) to generate neurons and intermediate progenitors (IPs). IPs populate the adjacent subventricular zone (SVZ) while neurons migrate through the intermediate zone (IZ) to populate specific layers within the cortical plate (CP). In humans, the organization of progenitor zones is markedly more elaborate; the SVZ is split by an inner fiber layer (IFL) into inner (ISVZ) and outer SVZ (OSVZ)[2]. The OSVZ represents an entirely separate progenitor layer populated by IPs and a unique stem cell termed outer radial glia (oRG)[3,4], which are only present to a limited degree in rodents[5]. Both the IFL and OSVZ are

Correspondence and requests for materials should be addressed to J.A.K. (juergen.knoblich@imba.oeaw.ac.at)..
Author Contributions: M.A.L and J.A.K. conceived of the project and experimental design and wrote the manuscript. M.A.L. performed experiments and analyzed data. M.R., C.-A.M., and D.W. performed experiments and analyzed data under supervision of J.A.K., J.M.P., and A.P.J. L.S.B., M.H., and T.H. performed patient diagnosis and provided MRIs coordinated by A.P.J. J.A.K. directed and supervised the project.

The authors declare no competing financial interests.

Europe PMC Funders Author Manuscripts

completely absent in mice[6]. These key differences allow for the striking expansion in neuronal output and brain size seen in humans[7,8].

Primary microcephaly (MCPH) is a neurodevelopmental disorder in which brain size is markedly reduced[9]. Autosomal recessive mutations have been identified in several genes, all of which encode proteins localizing to the mitotic spindle apparatus[10]. Heretofore, MCPH pathogenesis has primarily been examined in mouse models. However, mouse mutants for several of the known genes[11-14] have failed to recapitulate the severely reduced brain size seen in human patients.

Given the dramatic differences between mice and humans, methods that recapitulate paradigms of human brain development *in vitro* have enormous potential. While significant progress has been made for *in vitro* models of whole organ development for other systems, such as intestine[15], pituitary[16], and retina[17,18], a 3D culture model of the developing brain as a whole has not been established. Previous studies have modeled certain isolated neural tissues *in vitro*[19-23], including dorsal cerebral cortical tissue, which could recapitulate many aspects of early development. However, later events such as the formation of discrete cortical layers with stereotypic inside-out organization as well as human characteristics, such as the presence of oRG cells and the unique organization of progenitor zones, were not described.

Here, we describe a 3D culture system for deriving brain tissue *in vitro*. These so-called cerebral organoids develop a variety of regional identities organized as discrete domains capable of influencing one another. Furthermore, cerebral cortical regions display an organization similar to the developing human brain at early stages, as well as the presence of a considerable oRG population. Moreover, cerebral cortical neurons mature to form various pyramidal identities with modest spatial separation. Finally, we utilize patient-derived iPSCs and shRNA in these organoids to model CDK5RAP2 dependent pathogenesis of microcephaly, a disorder that has been difficult to model in mice.

Results

Generation of cerebral organoids

Recent progress with *in vitro* models of various organ systems has demonstrated the enormous self-organizing capacity for pluripotent stem cells to form whole tissues[15,18]. We built upon this concept and developed a protocol without the use of patterning growth factors, focusing instead on improving growth conditions and providing the environment necessary for intrinsic cues to influence development. We began with a modified approach to generate neuroectoderm from embryoid bodies[24]. Neuroectodermal tissues were then maintained in 3D culture and embedded in droplets of Matrigel to provide a scaffold for more complex tissue growth. These Matrigel droplets were then transferred to a spinning bioreactor to enhance nutrient absorption (Figure 1a). This method led to rapid development of brain tissues, which we termed cerebral organoids, requiring only 8-10 days for the appearance of neural identity and 20-30 days for defined brain regions to form.

Cerebral organoids at early stages (15-20 days) formed large, continuous neuroepithelia surrounding a fluid-filled cavity reminiscent of a ventricle with characteristic apical localization of the neural specific N-cadherin (Figure 1b). Furthermore, the neuroepithelium was larger and more continuous than tissues generated using a stationary approach[20], which instead formed an aggregate of several small rosette-like neuroepithelia (Figure 1b, Extended Data Figure 1a).

Although tissues reached maximal size by 2 months, cerebral organoids formed large (up to 4 mm in diameter), complex heterogeneous tissues, which could survive indefinitely (currently up to 10 months) when maintained in a spinning bioreactor. Histological and gross morphological analysis revealed regions reminiscent of cerebral cortex, choroid plexus, retina, and meninges (Figure 1c,d, Extended Data Figure 1b). Importantly, tissues typically reached a size limit likely due to the lack of a circulatory system and limitations in oxygen and nutrient exchange. Consistent with this, extensive cell death was visible in the core of these tissues (Extended Data Figure 1c), whereas the various brain regions developed along the exterior. Furthermore, cerebral organoids could be reproducibly generated with similar overall morphology and complexity from both human ES cells and induced pluripotent stem cells (iPSCs) (Extended Data Figure 1d, e).

Cerebral organoids display discrete brain regions

Brain development *in vivo* exhibits a striking degree of heterogeneity and regionalization as well as interdependency of various brain regions. Histological analysis suggested that human cerebral organoids might similarly display heterogeneous brain regions. To further examine this, we first tested the efficiency of initial neural induction in these tissues by performing RT-PCR for several markers of pluripotency and neural identity (Extended Data Figure 2a). As expected, pluripotency markers Oct4 and Nanog diminished during the course of organoid differentiation, while neural identity markers Sox1 and Pax6 were upregulated, indicating successful neural induction.

To test for early brain regionalization in whole organoids, we performed RT-PCR for forebrain (BF1 and Six3) and hindbrain (Krox20 and Isl1) markers (Figure 2a), revealing the presence of both populations within the tissue. However, as tissue development proceeded, forebrain markers remained highly expressed while hindbrain markers decreased, reminiscent of the developmental expansion of forebrain tissue during human brain development[25].

In order to test whether cells with these brain region identities developed as discrete regions within the organoids, as gross morphology would suggest, or were randomly interspersed within the tissue, we performed immunohistochemical staining for markers of forebrain, midbrain and hindbrain identities during early development of these tissues (16 days, Figure 2b, Extended Data Figure 2b). Pax6 expression revealed several regions of forebrain identity, and Otx1/2 expression marked forebrain/midbrain identity. These regions were located adjacent to regions lacking these markers but positive for hindbrain markers Gbx2, Krox20, and Pax2, which was reminiscent of the early midhindbrain boundary, suggesting similar regional communication and likely mutual repression.

In vivo brain development involves increasing refinement of regional specification. Therefore, we examined further developed cerebral organoid tissues for regional subspecification. We performed staining for the forebrain marker FoxG1 (Figure 2c), which labeled regions displaying typical cerebral cortical morphology. Many of these regions were also positive for Emx1 (Figure 2d), indicating dorsal cortical identity. We also tested for further subregionalization by staining for cortical lobe markers, namely Auts2, a marker of prefrontal cortex[26] (Figure 2e), Tshz2, a marker of the occipital lobe[26] (Extended Data Figure 2c), and Lmo4, a marker of frontal and occipital lobes but absent in parietal[26] (Extended Data Figure 2c). These markers could be seen in neurons labeling distinct regions of dorsal cortex, suggesting subspecification of cortical lobes.

Furthermore, staining for markers of hippocampus (Figure 2f) and ventral forebrain (Figure 2g), revealed specification of these regions, although they did not organize to form the overall structure seen *in vivo*. Strikingly, interneurons produced in ventral forebrain regions

exhibited a morphology and location consistent with migration from ventral to dorsal tissues (Extended Data Figure 2d). Within dorsal cortex, these neurons displayed neurites parallel to the apical surface, reminiscent of the migratory extensions seen in tangential migration *in vivo* (Figure 2h). Notably, Calretinin positive interneurons were absent from dorsal cortex of organoids lacking a ventral region (4/4 Nkx2.1 negative organoids), suggesting interneurons originate in ventral forebrain to migrate to the dorsal cortex. This suggests distant regions can influence one another in developing cerebral organoids.

Finally, other brain structures could be observed, namely choroid plexus (Figure 2i) and even immature retina (Figure 2j). Overall, all tissues examined displayed regions with dorsal cortical morphology (35/35, 100%), most displayed choroid plexus (25/35, 71%) and several displayed ventral forebrain identity as determined by Nkx2.1 immunoreactivity (12/35, 34%), whereas only a few displayed retinal tissue (determined by presence of retinal pigmented epithelium, 4/35, 11%). These results suggest that cerebral organoids developed a variety of brain region identities organized into discrete, though interdependent, domains.

Recapitulation of dorsal cortical organization

The most dramatic changes in brain evolution from rodent to human affect the dorsal cortex. Therefore, we analyzed the organization of dorsal cortical regions within cerebral organoids. Staining for markers of RGs and newborn neurons (Figure 3a) revealed typical organization into a layer reminiscent of the VZ with neurons located at the basal surface. Staining for Tbr1 (Figure 3b) revealed proper development of neural identity and radial migration to the developing preplate (precursor to CP) . Furthermore, staining for neural progenitor and neural specific BAF components revealed the characteristic switch in chromatin remodeling complexes during neural fate specification[27,28](Extended Data Figure 3a). Finally, staining for the IP marker Tbr2 (Figure 3c) revealed the presence of IPs adjacent to the VZ. Thus, dorsal cortical tissues displayed typical progenitor zone organization.

In both mice and humans, cortical progenitors undergo a stereotypical nuclear movement called interkinetic nuclear migration (IKNM). Mitotic divisions occur at the apical surface of the VZ while nuclei of cells in S-phase are located on the basal side of the VZ[29]. We stained for the mitotic marker phospho-histone H3 (PH3) (Figure 3d) and observed the majority of cells dividing at the apical surface. Similar observations were evident when we stained for phospho-Vimentin (Figure 3e), a marker of mitotic RGs. In addition, since this marker labels the entire cell, we could observe basal cellular processes typical of RGs, which extended to the outer surface of these tissues (Extended Data Figure 3b). Thus, RGs of cerebral organoids exhibited typical behavior and morphological features.

To examine this in more detail, we used a method to label individual RGs for morphology and live imaging experiments. In the mouse brain, individual cells can be labeled by *in utero* electroporation of fluorescent protein-expressing plasmids. Similarly, we injected GFP plasmid into fluid filled cavities of cerebral organoids and electroporated RGs adjacent to these ventricle-like cavities (Extended Data Figure 3c). This approach led to reproducible expression of GFP in RGs revealing typical morphology at various stages of development: early pseudostratified neuroepithelium (Extended Data Figure 3d) followed by later bipolar morphology with extended apical and basal processes (Extended Data Figure 3e, f).

To test for IKNM, we performed live imaging of GFP electroporated RGs in cerebral organoids and observed many examples of RGs that displayed movement of the cell body along the apical and basal processes (Figure 3f, Supplementary Video 1). Furthermore, we performed pulse-chase experiments with the S-phase marker BrdU (Figure 3g) and could observe a shift in RG nuclei from outer VZ localization towards the apical surface with time (Figure 3g).

RGs in the VZ of rodents exhibit biased spindle orientation, predominantly horizontal, parallel to the ventricular surface[30-33]. To examine whether RGs in human cerebral organoids exhibited a similar orientation bias, we used P-Vimentin staining to examine the plane of division in mitotic RGs (Extended Data Figure 3g). We observed mainly horizontal orientations (41%) (Figure 3h), somewhat similar to the orientation bias observed in other mammals. However, we also observed abundant oblique (37%) and vertical (22%) orientations, which were more abundant in these human tissues than has been described for rodent neocortex[30,31,34,35]. Interestingly, these measurements reflected the same trend recently described in the human brain[36], suggesting the cerebral organoids could recapitulate aspects of human cortical development.

We further examined the fate potential of these divisions to test whether organoid RGs could divide symmetrically and/or asymmetrically. We performed electroporation of GFP followed by a short 1-hour BrdU pulse and a 16-hour chase to lineage trace divisions of a small minority of cells. We examined double-labeled daughter cell pairs and could observe both symmetric proliferative fate outcomes, as well as asymmetric outcomes (Figure 3i). This suggests the RGs in these human tissues can undergo both symmetric and asymmetric divisions.

Formation of functional cerebral cortical neurons

The formation of the radially organized CP begins with the formation of its precursor, the preplate. To test for this initial organization, we stained 30-day organoids for Tbr1, a marker of the preplate[37], as well as Map2, a neuronal marker[38] (Figure 4a). This revealed the presence of a basal neural layer reminiscent of the preplate, and an apically adjacent region reminiscent of the IZ. Furthermore, we could observe Reelin positive neurons along the basal surface, suggesting the presence of Cajal-Retzius cells, an important population in generation of CP architecture[39].

The stereotypical layered structure of the mammalian CP is generated inside-out with later-born neurons migrating through existing layers to populate more superficial layers[40]. Although previous methods of deriving cortical neurons have been able to generate distinct layer identities[20,23,41], they have been unable to recapitulate this spatial separation. To test whether this organization could be recapitulated in cerebral organoids, we stained for cortical layer markers. In less developed tissues (30-day), early born Ctip2 neurons were located adjacent and internal to the $Tbr1^+$ preplate, suggesting initiation of CP layer formation (Extended Data Figure 4a). Furthermore, neurons exhibited rudimentary separation into early-born deep layer ($Ctip2^+$) and late-born superficial layer ($Satb2^+$ and $Brn2^+$) (Extended Data Figure 4b), which became more distinct as tissues developed (75-days) (Figure 4c). Finally, a cell-poor region reminiscent of the marginal zone was also evident (Extended Data Figure 1b). Importantly, although this modest spatial separation was an improvement upon other *in vitro* methods, organoids could not recapitulate the same degree of mature layer organization as *in vivo*, suggesting further cues are needed to generate the complex stereotypical layer II-VI organization.

In vivo, dorsal cortical neurons mature and extend long-range axons[42]. To test for these characteristics, we performed GFP electroporation and examined neuronal morphology. GFP-labeled axon projections displayed complex branching and growth cone behavior (Extended Data Figure 4c) and projected long-range axons in a manner reminiscent of axon bundling (Extended Data Figure 4d)[43].

Finally, we tested whether neurons within cerebral organoids could exhibited neural activity by performing calcium dye imaging to detect Ca^{2+} oscillations[44], which revealed spontaneous calcium surges in individual cells (Figure 4d, Extended Data Figure 4e and

Supplementary Videos 2, 3). Furthermore, we applied exogenous glutamate (Figure 4e) and observed more frequent calcium spikes, indicating glutamatergic receptor activity. Finally, we performed action potential blockade by application of tetrodotoxin (TTX) and observed dampened calcium surges indicating calcium spikes were dependent upon neuronal activity (Figure 4f).

Recapitulation of human cerebral cortical organization

Human brain development exhibits unique progenitor zone organization[2,7]. To test whether features of human brain development were recapitulated in cerebral organoids, we examined the distribution of $Sox2^+$ progenitors and observed a population displaced from the apical surface (Figure 5a, Extended Data Figure 5a) consistent with an oRG identity. Furthermore, these fairly abundant oRGs appeared separated from the apical VZ by a $Tuj1^+$ fiber layer (Figure 5a) reminiscent of the IFL. This organization suggests human cerebral organoids could recapitulate at least some aspects of human cortical development.

To rule out the possibility that this OSVZ-like organization was an *in vitro* artifact, we adapted the method to mouse ES cells to generate mouse cerebral organoids and examined whether a similar organization was present (Extended Data Figure 5b and c). We observed much smaller cortical tissues in mouse organoids compared with human, and only occasional oRGs that did not accumulate in an OSVZ-like region. These results suggest OSVZ and IFL-like layers are specific to human organoids.

We performed P-Vimentin staining to examine the morphology of human oRGs, which revealed basal processes but a lack of apical processes (Figure 5b), a hallmark of oRGs[3,4]. This suggests these basally displaced Sox2 and P-Vimentin positive progenitors indeed represent human oRGs. We also examined the division mode of oRGs and could identify daughter cell pairs in which only one daughter cell maintained Sox2 expression (Figure 5c) suggesting asymmetric division. Furthermore, we measured spindle orientation and found that the vast majority of oRGs divided vertically (Figure 5d). This division mode is remarkably similar to the findings recently described by LaMonica et al. in human brain slice cultures[36] suggesting recapitulation of human oRG behavior in cerebral organoids.

Cerebral organoids model human microcephaly

Since disorders affecting human brain development have often proved difficult to recapitulate in animal models, we tested whether organoids could be used to model neurodevelopmental disorders. We identified a patient with severe microcephaly (−13.2 s.d. below mean for age and sex, Figure 6a) and reduced stature (−6.7 s.d., Supplemental Text, Extended Data Figure 6a), who, as determined through exome sequencing and confirmed by capillary sequencing (Figure 6b), had compound heterozygous truncating mutations in *CDK5RAP2*. Skin fibroblasts from this patient revealed a loss of the CDK5RAP2 protein (Figure 6c, Extended Data Figure 6b) suggesting loss of function, consistent with previously reported *CDK5RAP2* mutations in primary microcephaly patients[45,46].

We performed reprogramming of patient skin fibroblasts using lentiviral delivery of the four well-described reprogramming factors: Oct4, Sox2, c-Myc, and Klf4[47,48]. We generated many independent clones of iPSCs and characterized four of these for morphology and pluripotency. All four lines exhibited similar doubling times and colony morphology that was indistinguishable from control iPSCs (Extended Data Figure 7a). All lines could form embryoid bodies and stained positive for the pluripotency marker alkaline phosphatase (Extended Data Figure 7b).

We performed cerebral organoid culture from all 4 lines and observed smaller EBs, which when transferred to neural induction failed to develop further (Extended Data Figure 7c).

We hypothesized that since the patient also displayed reduced stature, perhaps overall EB growth was perturbed. Therefore, in order to allow the EBs to develop to a comparable size as control, we modified the protocol slightly by increasing the initial iPSC number. This modification allowed for the formation of neuroectoderm and subsequent neural tissue for analysis, which revealed smaller neuroepithelial tissues and a large degree of neuronal outgrowth compared with control tissues (Figure 6d and Extended Data Figure 7d). Immunohistochemical staining for progenitors and neurons revealed smaller neural tissues with only very few progenitor regions (Figure 6e). These overall smaller neural tissues were reminiscent of the reduced brain size seen in the patient.

These patient-derived cerebral organoids provided a unique opportunity to examine the cause of the hypoplasia seen in microcephaly. We therefore examined an earlier stage (22 days) and observed that, whereas control tissues displayed abundant, large neuroepithelial tissues composed of progenitors, patient-derived tissues displayed only occasional neuroepithelial regions (Extended Data Figure 7e). Furthermore, these tissues displayed decreased RGs and increased neurons compared with control (Figure 6f, Extended Data Figure 7f) suggesting premature neural differentiation. To test this possibility, we performed BrdU pulse-chase experiments (Figure 6g) revealing a dramatic increase in the number of $BrdU^+/DCX^+$ cells in patient organoids, consistent with premature neurogenic non-proliferative divisions.

We furthermore examined radial glial spindle orientation and observed that, whereas control tissues at this early stage (22 days) displayed exclusively horizontal orientations (Figure 6h), patient organoids displayed many oblique and vertical oriented spindles (Figure 6h). These results could explain the patient tissue phenotype since precise horizontal orientation of the spindle is necessary for early symmetric expansion of neural stem cells[32].

Finally, we tested whether the phenotype could be rescued by reintroducing CDK5RAP2 protein. We performed coelectroporation of GFP and CDK5RAP2 into day 12 patient organoids and examined 6 days later. Since high overexpression of CDK5RAP2 was toxic (data not shown), the cells with high GFP signal did not survive to this time point. However, we could observe regions in CDK5RAP2 electroporated tissues with larger neuroepithelium compared with tissues electroporated only with GFP (Extended Data Figure 7g). This effect could be due to surviving cells with a low-level of CDK5RAP2 re-expression. Supporting this interpretation, staining for GFP (Extended Data Figure 7h) revealed many low-level GFP^+ cells in CDK5RAP2 coelectroporated patient organoids with radial glial morphology (54%±2 SEM, n=74 cells from 3 tissues). In contrast, GFP+ cells in patient organoids electroporated with GFP alone exhibited mainly neuronal morphology with significantly fewer radial glia (19%±11 SEM, n=102 cells from 3 tissues, $P<0.05$, Student's *t*-test). Thus, we conclude that the phenotype is specific to loss of CDK5RAP2.

As a further independent approach, we performed RNAi knockdown of CDK5RAP2 by coelectroporating GFP with two independent shRNAs found to knockdown endogenous CDK5RAP2 (Extended Data Figure 8a). Both shRNAs led to a striking loss of $Sox2^+$ progenitors and an increase in DCX^+ neurons (Figure 6i, Extended Data Figure 8b) reflecting a statistically significant increase in neuron production rather than progenitor maintenance (Extended Data Figure 8c). These findings support the conclusion that loss of CDK5RAP2 leads to premature neural differentiation at the expense of progenitors.

Discussion

We have established a novel approach to studying human neurodevelopmental processes through *in vitro* culture of cerebral organoids from human pluripotent stem cells. This

method recapitulates not only fundamental mechanisms of mammalian neurodevelopment, but also displays characteristics of human brain development. We are hopeful that this method will allow the study of a variety of neurodevelopmental processes specific to human brain development.

Furthermore, a primary goal in neuroscience is to understand the roots of human neurological disease. We have modeled at least some aspects of microcephaly in these cerebral organoids. The finding that progenitor zones in patient-derived tissues display premature neural differentiation at the expense of early progenitors supports a model in which the founder population of RG progenitors fails to properly expand in patient tissues, thereby leading to an overall smaller brain. This may also explain why mouse models have been unable to recapitulate the severity of the disorder in humans. It is hypothesized that the mouse founder population of neural progenitors do not undergo expansion to the same extent as in human before the onset of neurogenesis[7]. Thus, a disruption of the founder population in mice would not lead to as severe an effect as that seen in humans. Overall, our findings suggest we can utilize this *in vitro* culture system to model aspects of human neurodevelopment and neurological disease and hopefully provide novel insight into pathogenesis of these disorders.

Methods

Plasmid constructs and materials

GFP plasmid used for co-electroporation with shRNA and for live imaging was pCAG-GFP (Addgene plasmid 11150)[51]. shRNAs targeting human CDK5RAP2 were cloned using pSuper shRNA expression strategy (OligoEngine). Targeting sequences were as follows: shRNA 1 AGGACGTGTTGCTTCAGAAAT, shRNA 2 AGAGTCAGCCTTCTGCTAAAG, shRNA 3 GTGGAAGATCTCCTAACTAAA, shRNA 4 ACTATGAGACTGCTCTATCAG. The CDK5RAP2 expression construct was generated using the Gateway system (Invitrogen) by PCR amplification of CDK5RAP2 from MGC human CDK5RAP2 cDNA (clone ID: 9052276) using the primers with AttB sites: Forward: GGGGACAAGTTTGTACAAAAAAGCAGGCTTCATGATGGACTTGGTGTTGGAAG A, Reverse: GGGGACCACTTTGTACAAGAAAGCTGGGTCAGCTTTATTGGCTGAAAGTTCTTC TC. CDK5RAP2 was cloned into destination vector pcDNA3.1/nV5-DEST.

Cerebral organoid culture conditions

Human H9 ES (WA09) were obtained from WiCell at passage 26 with verified normal karyotype and contamination-free. iPS cells were obtained from System Biosciences (SC101A-1) verified pluripotent and contamination free. All human PSC lines were regularly checked and confirmed negative for mycoplasma. PSCs were maintained on CF-1 gamma irradiated MEFs (Global Stem) according to WiCell protocols. On day 0 of organoid culture, ESCs or iPSCs less than passage 50 were dissociated from MEFs by dispase treatment and MEFs were removed by gravity separation of stem cell colonies from MEFs before trypsinization of stem cells to generate single cells. 4500 cells were then plated in each well of an ultra-low binding 96-well plate (Corning) in hES media with low bFGF (5-fold reduced) and 50uM ROCK inhibitor[49] (Calbiochem).

EBs were fed every other day for 6 days then transferred to low adhesion 24-well plates (Corning) in neural induction media containing DMEM/F12, 1:100 N2 supplement (Invitrogen), Glutamax (Invitrogen), MEM-NEAA, and 1ug/ml Heparin[50] (Sigma). These began forming neuroepithelial tissues, which were fed every other day for 5 days. On Day 11 of the protocol, tissues were transferred to droplets of Matrigel (BD Biosciences) by

pipetting into cold Matrigel on a sheet of Parafilm with small 3mm dimples. These droplets were allowed to gel at 37C and were subsequently removed from the Parafilm and grown in differentiation media containing a 1:1 mixture of DMEM/F12 and Neurobasal containing 1:200 N2 supplement (Invitrogen), 1:100 B27 supplement without vitamin A (Invitrogen), 3.5ul/L 2-mercaptoethanol, 1:4000 insulin (Sigma), 1:100 Glutamax (Invitrogen), 1:200 MEM-NEAA.

After 4 days of stationary growth, the tissue droplets were transferred to a spinning bioreactor containing differentiation media as above except B27 supplement with vitamin A (Invitrogen) was used. Since retinoic acid has been shown to be important for neuronal differentiation *in vivo*[52], we included it in the final media used to differentiate the cerebral organoids.

Mouse organoid culture conditions

Mouse A9 ES cells were cultured on Mitomycin C growth inactivated MEFs and passaged according to standard protocols[53]. For the generation of mouse organoids, the organoid protocol was applied with the following modifications: cells were trypsinized and 2000 stem cells were plated in each well of an ultra-low binding 96-well plate in differentiation medium as described by Eiraku et al.[20] (Medium containing 10uM SB431542 but without Dkk-1). Subsequent steps were followed according to the human organoid method using identical media compositions, with the exception that for mouse tissues faster timing was used according to morphology. EBs were transferred to neural induction medium on day 4, embedded in matrigel droplets on day 6, and on day 9 transferred to the spinning bioreactor.

Organoid electroporation

Electroporation was performed using a petri dish tissue electrode and electro-square-porator (ECM 830) both from BTX Harvard Apparatus. A total of 3ul of 2ug/ul total plasmid (GFP for live imaging, 1.8ug/ul shRNA + 0.2ug/ul GFP for shRNA experiments) was injected in 4-5 locations within the organoid and electroporation was performed in differentiation media without antibiotics at 5 pulses, 80V, 50 ms duration, 1 sec interval. For rescue experiments, GFP expression plasmid and the CDK5RAP2 construct were coelectroporated at equal concentrations (1ug/ul each).

Live imaging in organoids

Live imaging was performed using a LSM780 confocal laser scanning system (Zeiss) equipped with temperature and CO2 control. For calcium imaging, Fluo-4 direct (Life Technologies) was prepared according to manufacturer and applied 60 min before the start of imaging. Imaging was performed at 494nm excitation and 516nm emission, frames taken every 20 sec for 100 frames. Data analysis of calcium imaging was performed using ImageJ (Fiji). Regions of interest (ROIs) were manually selected and mean fluorescence was calculated for each time frame. Change is fluorescence was calculated as follows: $\Delta F/F=(F-F_{basal}))/F_{background}$ where F_{basal} was the lowest mean fluorescence value across imaging while $F_{background}$ was the average mean fluorescence across all frames. Glutamate was added by bath application to media during imaging at a final concentration 100uM. TTX was added by bath application to media during imaging at a final concentration of 1uM and imaging was resumed after a 10min incubation time.

Histology and immunofluorescence

Tissues were fixed in 4% paraformaldehyde for 20 min at 4C followed by washing in PBS 3 times 10 min. Tissues were allowed to sink in 30% sucrose overnight and then embedded in 10%/7.5% gelatin/sucrose and cryosectioning at 20 μm. Tissue sections were stained with

hemotoxylin/eosin or used for immunostaining. For immunohistochemistry, section were blocked and permeabilized in 0.25% Triton-X, 4% normal donkey serum in PBS. Sections were then incubated with primary antibodies in 0.1% Triton-X, 4% normal donkey serum at the following dilutions: N-Cadherin (mouse, BD Biosciences 610920, 1:500), Sox2 (rabbit, Chemicon, AB5603, 1:300), Tuj1 (mouse, Covance MMS-435P, 1:750), TUNEL (In Situ Cell Death Detection Kit-Fluorescein, Roche), FoxG1 (rabbit, Abcam ab18259, 1:200), Emx1 (rabbit, Sigma HPA006421, 1:50), Krox20 (rabbit, Covance PRB-236P, 1:100), Pax2 (mouse, Abnova H00005076-M01, 1:200), Lmo4 (goat, Santa Cruz sc-11122, 1:50), Tshz2 (rabbit, Sigma SAB4500379, 1:50), Otx1+2 (rabbit, Abcam ab21990, 1:200), Gbx2 (goat, Santa Cruz sc22230, 1:100), Auts2 (rabbit, Sigma HPA000390, 1:250), Nkx2.1 (rabbit, Epitomics 6594-1, 1:250), Pax6 (mouse monoclonal, DSHB, 1:200), Pax6 (rabbit, Covance PRB-278P, 1:300), Calretinin (mouse, Swant 6B3, 1:100), Nrp2 (goat, RandD systems AF2215, 1:40), Fzd9 (rabbit, Acris SP4153P, 1:200), Prox1 (mouse, Chemicon MAB5654, 1:200), TTR (sheep, AbD Serotec AHP1837, 1:100), Tbr2 (rabbit, Chemicon AB9618, 1:500), Tbr1 (rabbit, Abcam ab31940, 1:300), MAP2 (mouse, 1:300), PH3 (rabbit, Cell Signaling Technology 9706S, 1:300), P-Vimentin (mouse, MBL International D076-3S, 1:250), BrdU (preincubation in 2N HCl 20min 37C, rat, AbD Serotec OBT0030CX, 1:500), Baf53a (rabbit, Bethyl IHC-00287, 1:250), Baf53b (rabbit, Abcam ab140642, 1:250), Reelin, (mouse, Millipore MAB5366, 1:200), Ctip2 (rat, Abcam ab18465, 1:100), Satb2 (rabbit, Abcam ab34735, 1:100), DCX (goat, Santa Cruz sc-8066, 1:300), Brn2 (goat, Santa Cruz sc-6029, 1:40). Secondary andibodies used were donkey AlexaFluor 488, 568, and 647 conjugates (Invitrogen, 1:500). For sections stained for BrdU, sections were first incubated with 2N HCl at 37C for 20 min followed by washing three times in PBS before blocking.

RT-PCR

Total mRNA samples were isolated from whole organoids or hES cells in triplicate using Trizol reagent (Invitrogen). Potential contaminating DNA was removed using DNA-Free (Ambion) and 1ug RNA was used for cDNA synthesis using SuperScript III (Life Technologies). PCR conditions and number of cycles (25-35 cycles) for each primer pair were empirically determined using hES cDNA or human fetal brain cDNA (Invitrogen). Cycles were run at 94C denaturation for 30 sec, 58-62C annealing for 45 sec, depending on primer pair, and 72C extension for 30 sec. Primer pairs used were as follows: Oct4a For ggagaagctggagcaaaacc, Rev tggctgaataccttcccaaa; Nanog For gatttgtgggcctgaagaaa, Rev ctttgggactggtggaagaa; Sox1 For tatcttctgctccggctgtt, Rev gggtcttcccttcctcctc; Pax6 For agttcttcgcaacctggcta, Rev attctctccccctccttcct; Actb For aaatctggcaccacaccttc, Rev agaggcgtacagggatagca; BF1 For aggagggcgagaagaagaac, Rev tgaactcgtagatgccgttg; Six3 For ctatcaacaaccccccaacca, Rev agccgtgcttgtcctagaaa; Krox20 For ttgaccagatgaacggagtg, Rev cttgcccatgtaagtgaaggt; Isl1 For gctttgttagggatgggaaa, Rev actcgatgtgatacaccttgga.

Cell culture and western blot

HEK293T cells were grown in 10% FBS/DMEM and split at 40% into a 6-well dish (BD Falcon) followed by transfection the next day using TurboFect (Thermo Scientific) with 5ug plasmid DNA. Cells were lysed 2 days later and western blot was performed using rabbit anti-CDK5RAP2 (A300-554A, Bethyl labs, 1:10,000) followed by blotting for mouse anti-alpha tubulin (mouse, Sigma T6199, 1:10,000). Dermal fibroblasts were obtained by skin punch biopsy and were cultured in amnioMAX C-100 complete medium (Invitrogen) and maintained in a 37°C incubator with 5% CO2 and 3% O2. Cells were lysed in 50 mM Tris-HCl pH 8, 280 mM NaCl, 0.5% NP40, 0.2 mM EDTA, 0.2 mM EGTA, 10% Glycerol supplemented with protease inhibitor tablet (Roche). Protein samples were run on a 3-8 % Tris-acetate gel (Invitrogen) followed by immunoblotting using rabbit anti-CDK5RAP2 (A300-554A, Bethyl labs, 1:2,000) and mouse anti-vinculin (V9264, Sigma, 1:2,000). To perform immunofluorescence, patient fibroblasts were fixed in −20°C methanol for 7 min

and then blocked in PBS/1 % bovine serum albumin. Cells were then incubated in rabbit anti-CDK5RAP2 (A300-554A, Bethyl labs, 1:2,000) and mouse anti-CPAP (SC-81432, Santa Cruz Biotechnology, 1:100) in blocking solution. Secondary antibodies used were donkey AlexaFluor 488 and 568 conjugates (Invitrogen, 1:500).

Research subject and gene identification

Genomic DNA was extracted from peripheral blood of Patient 3842 and the patient's parents by standard methods. Informed consent was obtained from the family and the study approved by the Multi-centre Research Ethics Committee for Scotland (04:MRE00/19). Whole exome capture and sequencing was performed at the Welcome Trust Sanger Institute (WTSI), UK. DNA was sheared to 150bp lengths by sonification (Covaris, Woburn, Massachusetts, USA) prior to whole exome capture and amplification using the SureSelect Human All Exon 50Mb kit (Agilent, Santa Clara, CA). Fragments were sequenced using the Illumina Hiseq platform. 76bp paired end sequence reads were aligned to the UCSC genome browser hg19 reference sequence using BWA. Sequence variants were obtained using GenomeAnalysisTK (www.broadinstitute.org/gatk/) and annotated with transcript and protein consequence, polyphen, condel and SIFT scores. Mutations were confirmed by bi-directional sequencing of PCR products using dye terminator chemistry on an ABI 3730 capillary sequencer (Applied Biosystems).

Patient iPSC reprogramming

Patient skin fibroblasts were reprogrammed using lentiviral delivery of Oct4, Sox2, Klf4, and c-Myc. Lentivirus production: A DNA mix consisting of virus packaging vectors (tat, rev, gag/pol, 1.5ug each, and vsv-g, 3ug) and the loxP flanked OKSM reprogramming vector (oct-4, klf4, sox2, c-myc, 30ug) were transfected into 293 cells. In brief, 112.5µl Fugene6 was added dropwise to 2ml DMEM under constant vortexing followed by a 10min incubation at RT. The DNA mix was added to the DMEM/Fugene6 mix while vortexing to generate the final transfection mix. After a 15min incubation at RT, the transfection mix was added onto 80% confluent 293 cells, cultured in 13ml 293 culture medium. Virus-containing medium was harvested and replaced with fresh medium 48h, 60h and 72h after transfection. The viral supernatant was stored at 4°C. Reprogramming of human dermal fibroblasts: 1×10^5 dermal fibroblasts were seeded the day before infection onto 10cm and 6cm 0.1% Gelatin-coated culture dishes. Cells were incubated for 12h with viral supernatant 1:1 mixed with dermal fibroblast medium supplemented with 4µg/ml polybrene. Thereafter, cells were washed with 1x PBS and cultured for 2 more days in dermal fibroblast medium. After 2 days medium was switched to human iPSCs medium supplemented with 10ng/ml bFGF (peprotech, cat.nr: 100-18B), 10µM CHIR99021 (stemgent, cat.nr: 04-0004) and 1µM PD 0325901 (stemgent, cat.nr: 04-0006) and cells cultured for 21 days. Medium was changed every day. Outgrowing colonies, identified by morphological appearance, were picked and passaged on inactivated CF-1 MEFs (global stem, cat.nr: GSC-6201M). Patient derived iPS lines were compared to control iPS cells obtained from a healthy donor (System Biosciences, SC101A-1). Alkaline phosphatase staining was performed using Vector Blue Alkaline Phosphatase Substrate Kit (Vector Laboratories, SK5300). Quantifications in patient and control iPSC derived organoids were performed blinded using coded file names in ImageJ.

Supplementary Text

Patient clinical synopsis

Patient A3842 exhibited growth restriction from fetal life, with marked reduction in brain size evident at 22/40 weeks gestation. Pregnancy progressed otherwise normally and the patient was born at term weighing 1.82kg (−3.9 s.d.). Postnatally, growth was also reduced

such that height at 3 years 7 months was 73 cm (−6.7 s.d.), and head circumference 35cm (−13.2 s.d.), in keeping with a severe disproportionate microcephaly. The patient had quite prominent eyes and conical shaped wide-space teeth, but was otherwise unremarkable on examination. No neurological deficits or malformations in other systems were evident, aside from a mixed conductive/sensorineural hearing loss. Development milestones were mildly/moderately delayed. Neuroimaging at 22/40 gestation demonstrated a smooth brain (the Sylvian fissure normally evident at this gestation was not present) with small frontal lobes and partial absence of the corpus callosum. Postnatally, MRI demonstrated microcephaly with a simplified gyral pattern and a cerebral cortex of normal thickness. In summary, clinical findings were in keeping with previous cases of CDK5RAP2 primary microcephaly (deafness has been previously reported with CDK5RAP2[45,46]), with growth parameters falling on the primary microcephaly-microcephalic primordial dwarfism spectrum reported for other centrosomal microcephaly genes such as *CENPJ* and *CEP152*[45,54-56].

Supplementary Material

Refer to Web version on PubMed Central for supplementary material.

Acknowledgments

We are grateful to members of the Knoblich lab for technical expertise and feedback and to Angela Peer, Paul Moeseneder, and Nina Corsini for experimental support and Marko Repic for help with establishing organoid electroporations. We also thank the Stem Cell and BioOptics core facilities of IMBA/IMP for technical support. We would especially like to thank the patient and their family for participation in this study. We would also like to thank Simon McGurk for providing control MRI images. M.A.L. received funding from an EMBO post-doctoral fellowship and a Helen Hay Whitney post-doctoral fellowship. Work in A.P.J.'s laboratory is supported by the Medical Research Council, a starter grant from the ERC and the Lister Institute for Preventative Medicine. This research was also supported in part by Wellcome Trust grant WT098051. Work in J.A.K.'s laboratory is supported by the Austrian Academy of Sciences, the Austrian Science Fund (FWF) (projects Z153-B09 and I552-B19), and an advanced grant from the European Research Council (ERC).

References

1. Götz M, Huttner WB. The cell biology of neurogenesis. Nat Rev Mol Cell Biol. 2005; 6:777–788. [PubMed: 16314867]
2. Zecevic N, Chen Y, Filipovic R. Contributions of cortical subventricular zone to the development of the human cerebral cortex. J. Comp. Neurol. 2005; 491:109–122. [PubMed: 16127688]
3. Fietz SA, et al. OSVZ progenitors of human and ferret neocortex are epithelial-like and expand by integrin signaling. Nat Neurosci. 2010; 13:690–699. [PubMed: 20436478]
4. Hansen DV, Lui JH, Parker PRL, Kriegstein AR. Neurogenic radial glia in the outer subventricular zone of human neocortex. Nature. 2010; 464:554–561. [PubMed: 20154730]
5. Smart IHM, Dehay C, Giroud P, Berland M, Kennedy H. Unique morphological features of the proliferative zones and postmitotic compartments of the neural epithelium giving rise to striate and extrastriate cortex in the monkey. Cereb. Cortex. 2002; 12:37–53. [PubMed: 11734531]
6. Shitamukai A, Konno D, Matsuzaki F. Oblique radial glial divisions in the developing mouse neocortex induce self-renewing progenitors outside the germinal zone that resemble primate outer subventricular zone progenitors. J Neurosci. 2011; 31:3683–3695. [PubMed: 21389223]
7. Lui JH, Hansen DV, Kriegstein AR. Development and evolution of the human neocortex. Cell. 2011; 146:18–36. [PubMed: 21729779]
8. Fietz SA, Huttner WB. Cortical progenitor expansion, self-renewal and neurogenesis-a polarized perspective. Curr Opin Neurobiol. 2011; 21:23–35. [PubMed: 21036598]
9. Cox J, Jackson AP, Bond J, Woods CG. What primary microcephaly can tell us about brain growth. Trends Mol Med. 2006; 12:358–366. [PubMed: 16829198]
10. Megraw TL, Sharkey JT, Nowakowski RS. Cdk5rap2 exposes the centrosomal root of microcephaly syndromes. Trends Cell Biol. 2011; 21:470–480. [PubMed: 21632253]

11. Barrera JA, et al. CDK5RAP2 regulates centriole engagement and cohesion in mice. Dev Cell. 2010; 18:913–926. [PubMed: 20627074]
12. Lizarraga SB, et al. Cdk5rap2 regulates centrosome function and chromosome segregation in neuronal progenitors. Development. 2010; 137:1907–1917. [PubMed: 20460369]
13. Pulvers JN, et al. Mutations in mouse Aspm (abnormal spindle-like microcephaly associated) cause not only microcephaly but also major defects in the germline. Proc Natl Acad Sci USA. 2010; 107:16595–16600. [PubMed: 20823249]
14. Gruber R, et al. MCPH1 regulates the neuroprogenitor division mode by coupling the centrosomal cycle with mitotic entry through the Chk1-Cdc25 pathway. Nat. Cell Biol. 2011; 13:1325–1334. [PubMed: 21947081]
15. Sato T, et al. Single Lgr5 stem cells build crypt-villus structures in vitro without a mesenchymal niche. Nature. 2009; 459:262–265. [PubMed: 19329995]
16. Suga H, et al. Self-formation of functional adenohypophysis in three-dimensional culture. Nature. 2011; 480:57–62. [PubMed: 22080957]
17. Nakano T, et al. Self-formation of optic cups and storable stratified neural retina from human ESCs. Cell Stem Cell. 2012; 10:771–785. [PubMed: 22704518]
18. Eiraku M, et al. Self-organizing optic-cup morphogenesis in three-dimensional culture. Nature. 2011; 472:51–56. [PubMed: 21475194]
19. Eiraku M, Sasai Y. Self-formation of layered neural structures in three-dimensional culture of ES cells. Curr Opin Neurobiol. 2012; 22:768–777. [PubMed: 22405989]
20. Eiraku M, et al. Self-organized formation of polarized cortical tissues from ESCs and its active manipulation by extrinsic signals. Cell Stem Cell. 2008; 3:519–532. [PubMed: 18983967]
21. Danjo T, et al. Subregional specification of embryonic stem cell-derived ventral telencephalic tissues by timed and combinatory treatment with extrinsic signals. J Neurosci. 2011; 31:1919–1933. [PubMed: 21289201]
22. Muguruma K, et al. Ontogeny-recapitulating generation and tissue integration of ES cell-derived Purkinje cells. Nat Neurosci. 2010; 13:1171–1180. [PubMed: 20835252]
23. Mariani J, et al. Modeling human cortical development in vitro using induced pluripotent stem cells. Proc Natl Acad Sci USA. 2012; 109:12770–12775. [PubMed: 22761314]
24. Xia X, Zhang S-C. Differentiation of neuroepithelia from human embryonic stem cells. Methods Mol Biol. 2009; 549:51–58. [PubMed: 19378195]
25. Swanson LW. Mapping the human brain: past, present, and future. Trends Neurosci. 1995; 18:471–474. [PubMed: 8592750]
26. Bedogni F, et al. Tbr1 regulates regional and laminar identity of postmitotic neurons in developing neocortex. Proc Natl Acad Sci USA. 2010; 107:13129–13134. [PubMed: 20615956]
27. Yoo AS, et al. MicroRNA-mediated conversion of human fibroblasts to neurons. Nature. 2011; 476:228–231. [PubMed: 21753754]
28. Lessard J, et al. An essential switch in subunit composition of a chromatin remodeling complex during neural development. Neuron. 2007; 55:201–215. [PubMed: 17640523]
29. Willardsen MI, Link BA. Cell biological regulation of division fate in vertebrate neuroepithelial cells. Dev. Dyn. 2011; 240:1865–1879. [PubMed: 21761474]
30. Chenn A, McConnell SK. Cleavage orientation and the asymmetric inheritance of Notch1 immunoreactivity in mammalian neurogenesis. Cell. 1995; 82:631–641. [PubMed: 7664342]
31. Konno D, et al. Neuroepithelial progenitors undergo LGN-dependent planar divisions to maintain self-renewability during mammalian neurogenesis. Nat. Cell Biol. 2008; 10:93–101. [PubMed: 18084280]
32. Yingling J, et al. Neuroepithelial stem cell proliferation requires LIS1 for precise spindle orientation and symmetric division. Cell. 2008; 132:474–486. [PubMed: 18267077]
33. Postiglione MP, et al. Mouse inscuteable induces apical-basal spindle orientation to facilitate intermediate progenitor generation in the developing neocortex. Neuron. 2011; 72:269–284. [PubMed: 22017987]

34. Smart IH. Proliferative characteristics of the ependymal layer during the early development of the mouse neocortex: a pilot study based on recording the number, location and plane of cleavage of mitotic figures. J. Anat. 1973; 116:67–91. [PubMed: 4777782]
35. Zamenhof S. Quantitative studies of mitoses in fetal rat brain: orientations of the spindles. Brain Res. 1987; 428:143–146. [PubMed: 3815110]
36. Lamonica BE, Lui JH, Hansen DV, Kriegstein AR. Mitotic spindle orientation predicts outer radial glial cell generation in human neocortex. Nat Commun. 2013; 4:1665. [PubMed: 23575669]
37. Hevner RF, et al. Tbr1 regulates differentiation of the preplate and layer 6. Neuron. 2001; 29:353–366. [PubMed: 11239428]
38. Shafit-Zagardo B, Kalcheva N. Making sense of the multiple MAP-2 transcripts and their role in the neuron. Mol. Neurobiol. 1998; 16:149–162. [PubMed: 9588626]
39. Frotscher M. Cajal-Retzius cells, Reelin, and the formation of layers. Curr Opin Neurobiol. 1998; 8:570–575. [PubMed: 9811621]
40. Tsai L-H, Gleeson JG. Nucleokinesis in neuronal migration. Neuron. 2005; 46:383–388. [PubMed: 15882636]
41. Gaspard N, et al. An intrinsic mechanism of corticogenesis from embryonic stem cells. Nature. 2008; 455:351–357. [PubMed: 18716623]
42. De Carlos JA, O'Leary DD. Growth and targeting of subplate axons and establishment of major cortical pathways. J Neurosci. 1992; 12:1194–1211. [PubMed: 1556593]
43. Chédotal A. Further tales of the midline. Curr Opin Neurobiol. 2011; 21:68–75. [PubMed: 20724139]
44. Sato TR, Gray NW, Mainen ZF, Svoboda K. The functional microarchitecture of the mouse barrel cortex. PLoS Biol. 2007; 5:e189. [PubMed: 17622195]
45. Bond J, et al. A centrosomal mechanism involving CDK5RAP2 and CENPJ controls brain size. Nat Genet. 2005; 37:353–355. [PubMed: 15793586]
46. Pagnamenta AT, et al. A novel nonsense CDK5RAP2mutation in a Somali child with primary microcephaly and sensorineural hearing loss. Am. J. Med. Genet. 2012; 158A:2577–2582. [PubMed: 22887808]
47. Takahashi K, Yamanaka S. Induction of pluripotent stem cells from mouse embryonic and adult fibroblast cultures by defined factors. Cell. 2006; 126:663–676. [PubMed: 16904174]
48. Okita K, Ichisaka T, Yamanaka S. Generation of germline-competent induced pluripotent stem cells. Nature. 2007; 448:313–317. [PubMed: 17554338]
49. Watanabe K, et al. A ROCK inhibitor permits survival of dissociated human embryonic stem cells. Nat. Biotechnol. 2007; 25:681–686. [PubMed: 17529971]
50. Hu B-Y, Zhang S-C. Directed differentiation of neural-stem cells and subtype-specific neurons from hESCs. Methods Mol Biol. 2010; 636:123–137. [PubMed: 20336520]
51. Matsuda T, Cepko CL. Electroporation and RNA interference in the rodent retina in vivo and in vitro. Proc Natl Acad Sci USA. 2004; 101:16–22. [PubMed: 14603031]
52. Siegenthaler JA, et al. Retinoic acid from the meninges regulates cortical neuron generation. Cell. 2009; 139:597–609. [PubMed: 19879845]
53. Tremml G, Singer M, Malavarca R. Culture of mouse embryonic stem cells. Curr Protoc Stem Cell Biol. 2008 Chapter 1, Unit 1C.4.
54. Al-Dosari MS, Shaheen R, Colak D, Alkuraya FS. Novel CENPJ mutation causes Seckel syndrome. J. Med. Genet. 2010; 47:411–414. [PubMed: 20522431]
55. Kalay E, et al. CEP152 is a genome maintenance protein disrupted in Seckel syndrome. Nat Genet. 2011; 43:23–26. [PubMed: 21131973]
56. Guernsey DL, et al. Mutations in centrosomal protein CEP152 in primary microcephaly families linked to MCPH4. Am J Hum Genet. 2010; 87:40–51. [PubMed: 20598275]

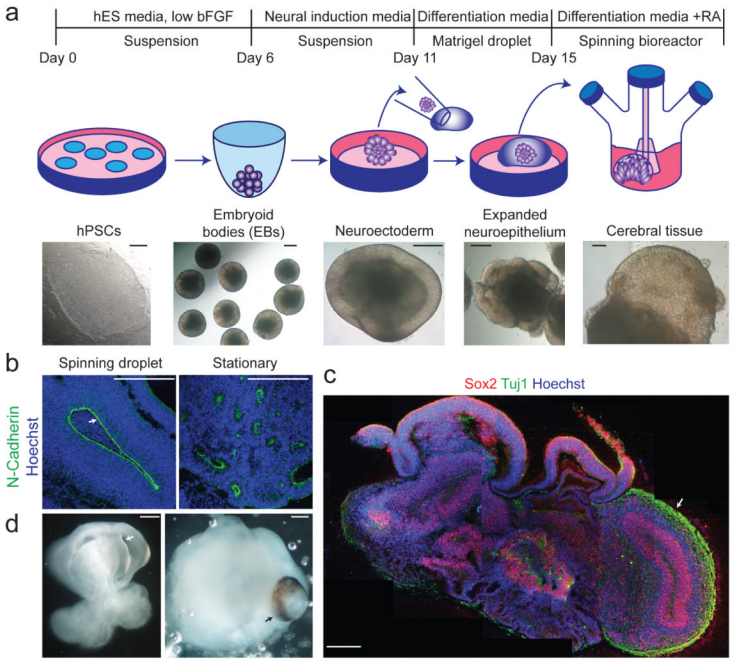

Figure 1. Description of cerebral organoid culture system

a, Schematic of the culture system described in detail in Methods. Example images of each stage are shown. **b,** Neuroepithelial tissues generated using this approach (left panel) exhibited large fluid-filled cavities and typical apical localization of the neural N-cadherin (arrow). These tissues were larger and more continuous than tissues grown in stationary suspension without Matrigel (right panel). **c,** Sectioning and immunohistochemistry revealed complex morphology with heterogeneous regions containing neural progenitors (Sox2, red) and neurons (Tuj1, green) (arrow). **d,** Low magnification bright field images revealing fluid-filled cavities reminiscent of ventricles (white arrow) and retina tissue, as indicated by retinal pigmented epithelium (black arrow). Scale bars: 200 μm.

Europe PMC Funders Author Manuscripts

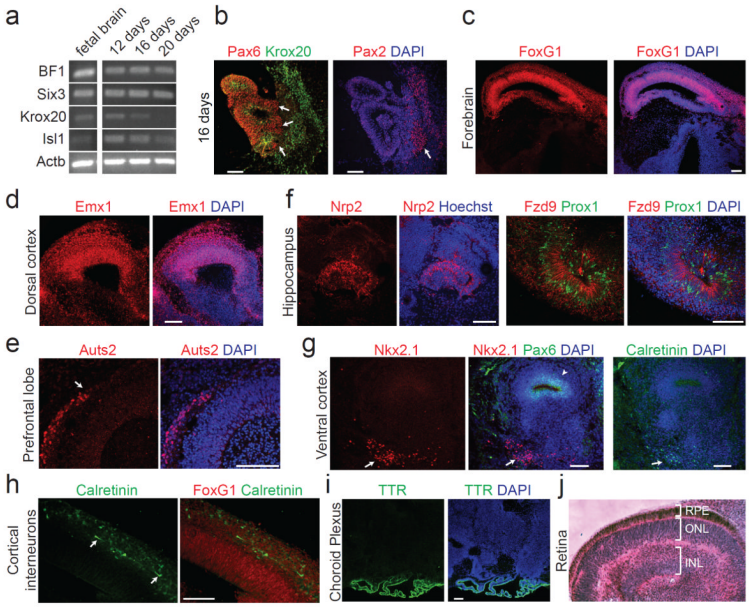

Figure 2. Human cerebral organoids recapitulate various brain region identities

a, RT-PCR for forebrain markers (BF1 and Six3) and hindbrain markers (Krox20 and Isl1) at 12, 16 and 20 days of differentiation. Human fetal brain cDNA was used as positive control. **b,** Immunohistochemistry in serial sections for the forebrain marker Pax6 (red, first panel) and the hindbrain markers Krox20 (green, first panel) and Pax2 (red, second panel) at 16 days of differentiation. Note the juxtaposition reminiscent of the mid-hindbrain boundary (arrows). DAPI marks nuclei (blue). **c,-i,** Staining for various brain region identities: forebrain, FoxG1 (**c**); dorsal cortex, Emx1 (**d**); prefrontal cortex (note the discrete boundary, arrow), Auts2 (**e**); hippocampus, Nrp2, Fzd9, Prox1 (**f**); ventral forebrain, Nkx2.1 (**g**) and choroid plexus, TTR (**i**). **g,** Staining for adjacent ventral (arrow) and dorsal (Pax6, arrowhead) forebrain and for calretinin (green) in a serial section revealing cortical interneurons in the ventral region (arrow). Calretinin interneurons within dorsal cortex (**h**) exhibit typical morphology of tangential migration (arrows). **j,** Hematoxylin-eosin staining of retinal tissue exhibiting stereotypical layering: retinal pigment epithelium (RPE), outer nuclear layer (ONL) and inner nuclear layer (INL). Scale bars: 100 μm.

Europe PMC Funders Author Manuscripts

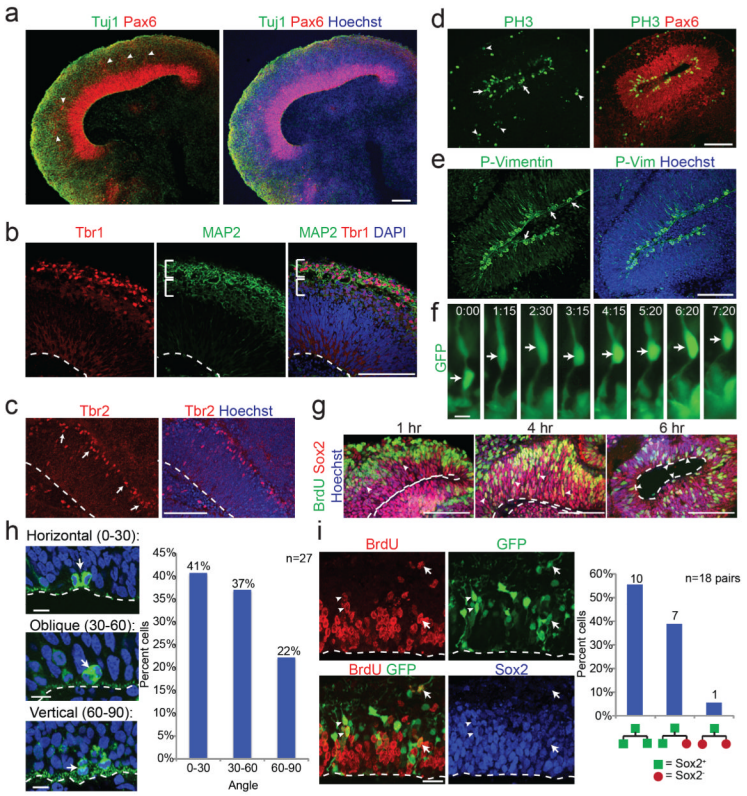

Figure 3. Stereotypical organization and behavior of progenitors

a, Immunohistochemistry for neurons (Tuj1, green) and RGs (Pax6, red) in a large dorsal cortical region. Note the additional Pax6^{+} RGs located outside the VZ (arrowheads), reminiscent of oRGs. **b,** Staining for the preplate marker Tbr1 (red) and neuronal marker MAP2 (green) revealing superficial preplate (upper bracket) and underlying neuronal IZ-like layer (lower bracket). **c,** Staining for the IP marker Tbr2 (red) revealing SVZ localization of IPs (arrows). **d,** Staining for phospho-histone H3 (PH3, green) to mark radial glia (Pax6^{+}) in mitosis. Arrows mark apical surface divisions; arrowheads mark SVZ divisions. **e,** Phospho-Vimentin (green) staining for mitotic radial glia which primarily divide at the apical surface (arrows). **f,** Frames from live imaging of GFP electroporated radial glia showing cell body movement (arrow). Time shown in hrs:min. **g,** BrdU pulse-chase revealing progressive IKNM of BrdU labeled nuclei (green, arrowheads) from basal VZ (1hr) to more apical position (4-6hr). **h,** Quantification of radial glial division orientation displayed in bins of 0-30 (horizontal), 30-60 (oblique) and 60-90 degrees (vertical). n=27 anaphase cells from 5 cerebral cortical tissues. **i.** Lineage tracing in GFP electroporated and BrdU pulsed tissues to mark daughter cell pairs following 16-hr chase revealing symmetric (arrowheads) and asymmetric (arrows) fates indicated by Sox2 staining (blue). Quantification for 18 cell pairs from three cortical tissues. Numbers above bars are absolute cell numbers. Dashed line indicates apical surface (**b, c, g, i**). Scale bars: 100 μm (**a-e,g**), 10 μm (**f, h**), 20 μm (**i**).

Europe PMC Funders Author Manuscripts

Europe PMC Funders Author Manuscripts

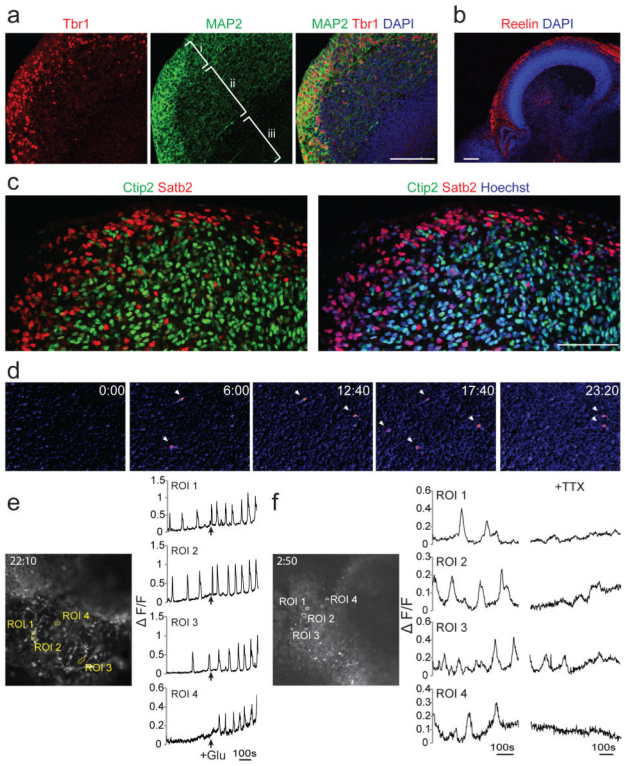

Figure 4. Organization and maturation of cerebral cortical neurons

a, Immunohistochemical staining at day 30 showing preplate (Tbr1) with early signs of radial organization (MAP2, bracket i) and the presence of an IZ-like layer (bracket ii) adjacent to the VZ/SVZ (bracket iii). DAPI marks nuclei (blue). **b,** Reelin staining indicating Cajal-Retzius cells along the basal surface of dorsal cortical tissue. **c,** Staining for early born (Ctip2) and late born (Satb2) neurons at 75 days differentiation reveals separation and rudimentary inside-out organization. **d.** False color heat map frames from Fluo-4 calcium live imaging revealing spontaneous calcium surges (arrowheads). Time is displayed in min:sec. **e.** Single cell tracings of calcium surges with glutamate application (regions of interest, ROI, outlined in left panel) as measured by change in fluorescence (arbitrary units). Arrows mark the time of addition of glutamate. **f.** Single cell tracing (ROIs marked in image at left) of calcium surges before (left panels) and after the addition of TTX (right panels). Scale bars: 100 μm.

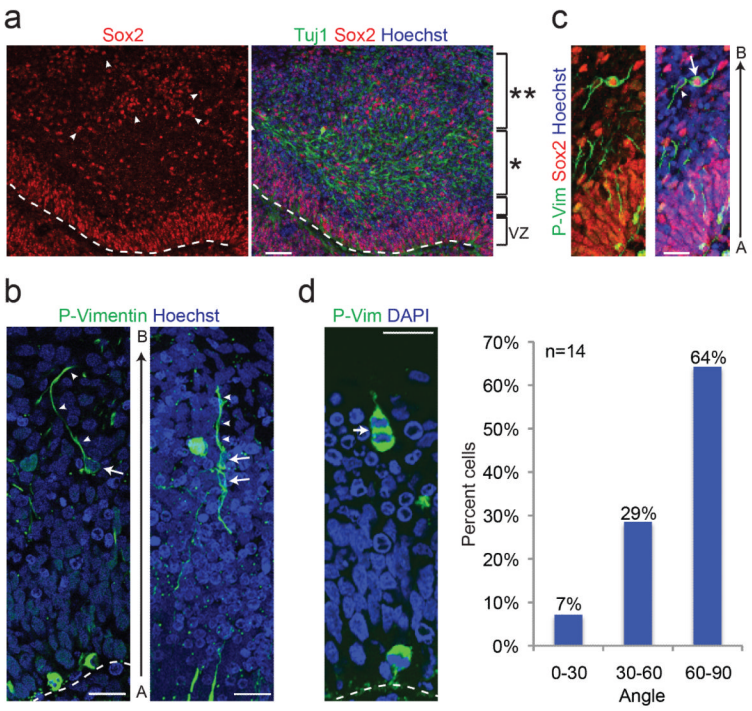

Figure 5. Cerebral organoids produce oRGs with typical morphology and behavior

a. Immunohistochemical staining for RGs (Sox2) and neuronal processes (Tuj1) reveals the presence of oRGs (arrowheads) organized similar to human cortical development (OSVZ-like layer, ** bracket) separated from the VZ by a layer of $Tuj1^+$ fibers similar to IFL (* bracket). **b.** Staining for phospho-Vimentin revealing dividing oRGs (arrows) with typical morphology: possessing a basal process (arrowheads) but lacking an apical process. Right panel: a daughter cell pair showing unequal inheritance of the basal process. Apical-basal orientation indicated by "A→B". **c.** Staining for phospho-Vimentin (P-Vim) in a recently divided daughter cell pair with asymmetric fates: one oRG (arrow, $Sox2^+$) while the other lacks Sox2 expression (arrowhead). **d.** Orientation of division of a mitotic oRG in anaphase revealing vertical (60-90 degrees) orientation relative to the apical surface (dashed line). Quantification of spindle orientation for 14 anaphase oRGs from 6 different cortical tissues. Scale bars: 50 μm (**a**), 20 μm (**b**-**d**).

Europe PMC Funders Author Manuscripts

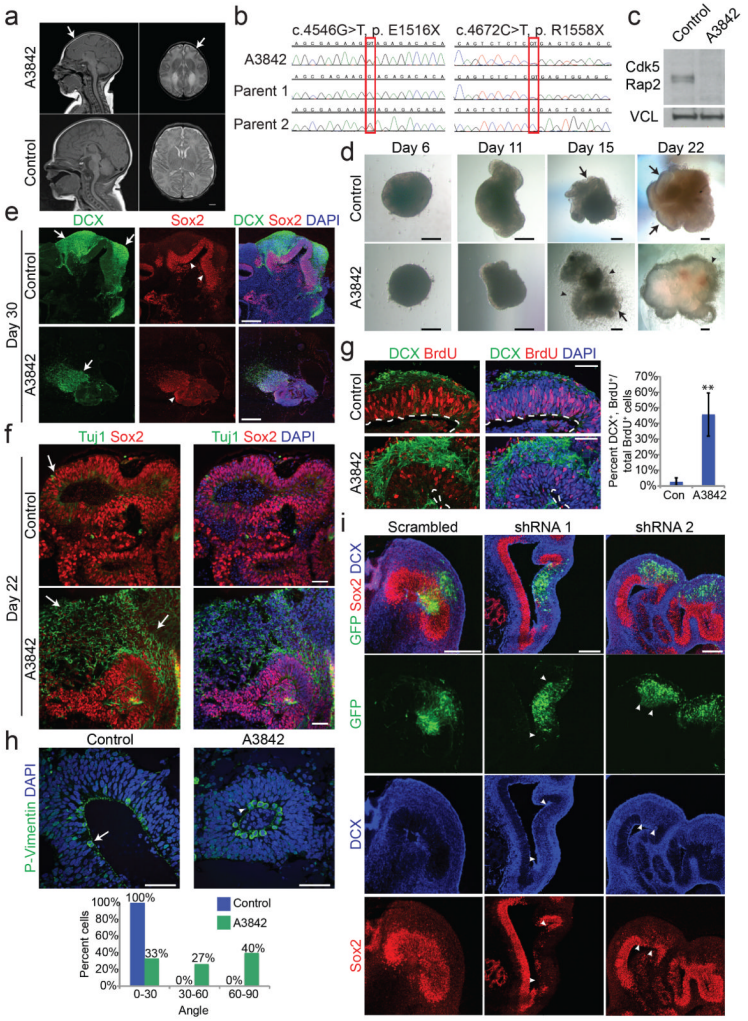

Figure 6. Cerebral organoid modeling of microcephaly

a. MRI scan from patient A3842 taken at birth (top) compared with age-matched control (bottom) showing brain and head size reduction and simplified cortical folding (arrows). Saggital T1 (left) and axial T2 (right) images. Scale bar 1cm. **b.** Sequencing chromatograms demonstrating compound heterozygous nonsense mutations inherited from each parent. **c.** CDK5RAP2 protein is undetectable on immunoblotting of patient cell lysate (A3842) compared with control skin fibroblasts. Vinculin (VCL), loading control. **d.** Representative bright-field images of control and patient-derived cerebral organoids (A3842 line 1M, all lines shown in Extended Data Figure 7d) at 6, 11, 15, and 22 days of differentiation. Control exhibits large fluid-filled cortical regions (arrows), while patient-derived exhibits increased outgrowth (arrowheads). **e.** Immunohistochemistry in control and patient-derived (10M) tissues at day 30 of differentiation revealing fewer neurons (Doublecortin, DCX, arrows) and smaller progenitor zones (Sox2, arrowheads). **f.** Staining at day 22 showing increased neurons (Tuj1, arrows) in patient-derived tissue (14B). **g.** BrdU pulse-chase in control and patient-derived organoids (14B) showing higher percentage of $BrdU^+$ cells with neural identity and less in the VZ compared with control. Results quantified at right. Error bars are S.D. $^{**}P<0.01$, Student's *t*-test. n=3 organoids for each condition (300 cells total for control, 204 cells for patient). **h.** P-Vimentin staining in control and patient-derived tissues (14B)

Europe PMC Funders Author Manuscripts

showing RG mitotic divisions. Control RGs at anaphase divided exclusively horizontal (0-30 degree angle, arrow) whereas patient RGs displayed many oblique and vertical orientations (arrowhead). Results quantified at right ($P<0.01$, 2×3 Fisher's exact test, n=11 cells for control, n=15 cells for patient-derived, from >5 cortical regions each). **i.** hESC organoids co-electroporated with GFP and scrambled or CDK5RAP2 shRNAs and examined after 5 days. Electroporated regions (demarcated by arrowheads) exhibit loss of $Sox2^+$ progenitors and increased Doublecortin (DCX) neurons. Scale bars: 200 μm (**d, e, i**), 50 μm (**f-h**).

Europe PMC Funders Author Manuscripts